Nanostructured Materials for Thermoelectric Energy Conversion and Sensor Applications

Li Shi

Associate Professor

Department of Mechanical Engineering &

Texas Materials Institute

The University of Texas at Austin

Outline

- Thermoelectrics of bulk and nanostructured materials
- Probing local thermopower of quantum wells
- Thermoelectric characterizations of individual nanowires using nanofabricated devices
- Integration of metal oxide nanowires with microsystems for nerve agent detection

Outline

- Thermoelectrics of bulk and nanostructured materials

- Probing local thermopower of quantum wells

- Thermoelectric characterizations of individual nanowires using nanofabricated devices

- Integration of metal oxide nanowires with microsystems for nerve agent detection

Thermoelectric Power Generation

- Seebeck effect:

$$S = \frac{V}{\Delta T}$$

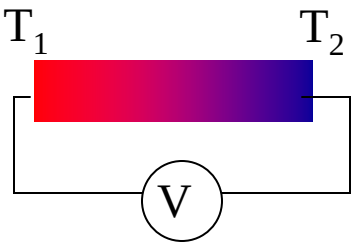

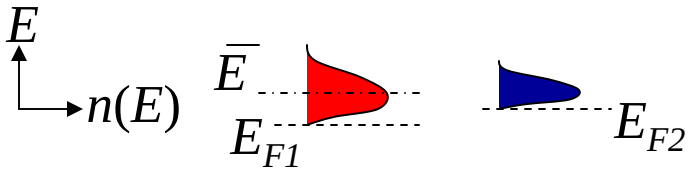

$$|S| \approx \frac{(\bar{E} - E_F)}{eT}$$

- Thermoelectric power generator:

-- No moving parts
-- Quiet

- **Radioisotope thermoelectric generator in NASA deep space probes**

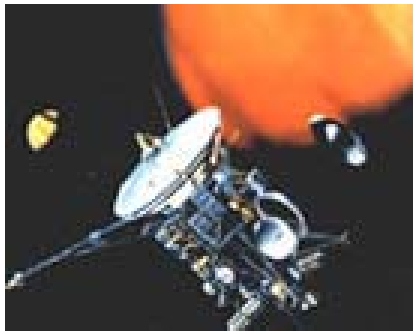

- **Waste heat recovery from automobiles (DOE Project Freedom Car)**

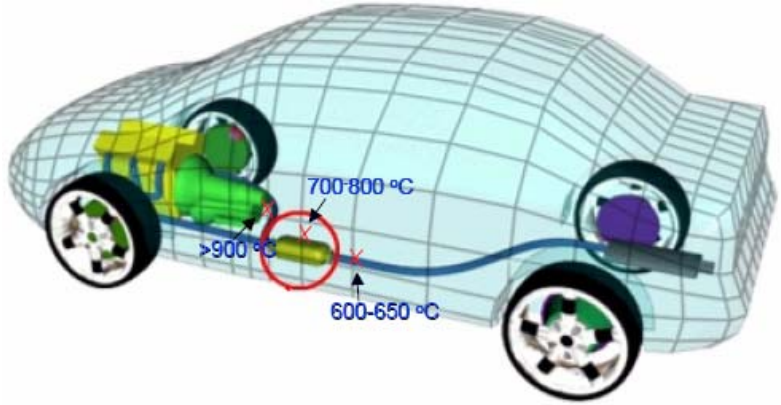

- **All electric ships (NAVY Seapower 21)**

Thermoelectric Cooling Performance

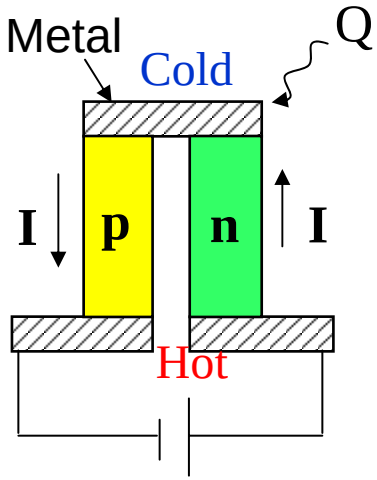

- **Coefficient of Performance (COP ≡ Q/IV)**

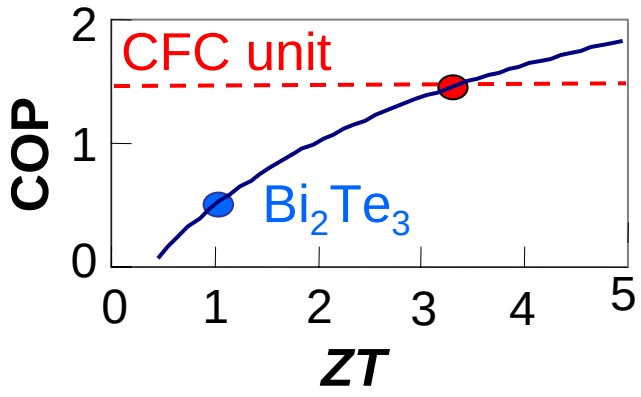

- ***ZT*: Figure of Merit**

Seebeck coefficient

Electrical conductivity

$$ZT \equiv \frac{S^2\sigma}{\kappa} T$$

Thermal conductivity

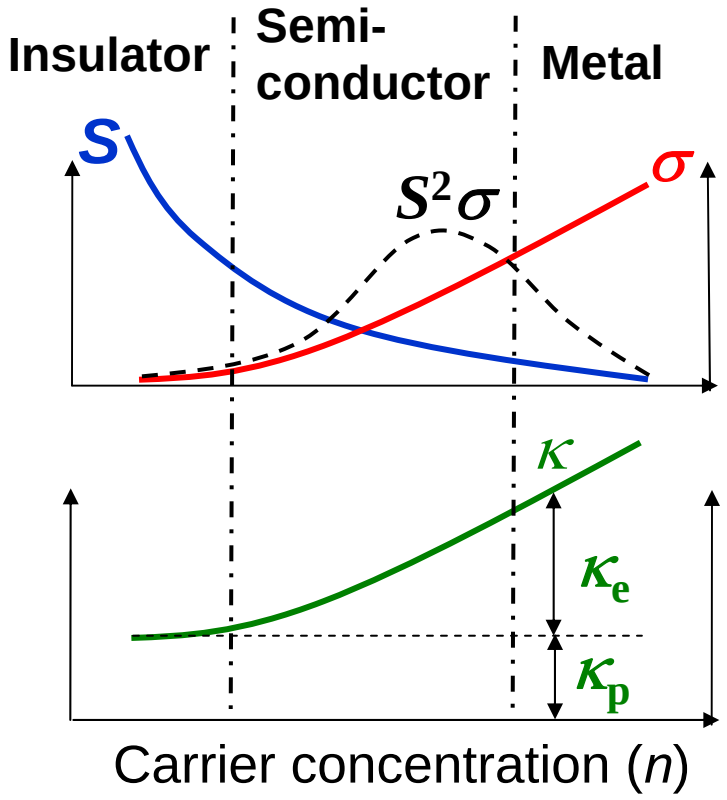

Size Effects on Thermoelectric Properties

Solids	Dominant energy carriers
Metals:	Electrons
Insulators:	Phonons (crystal waves)

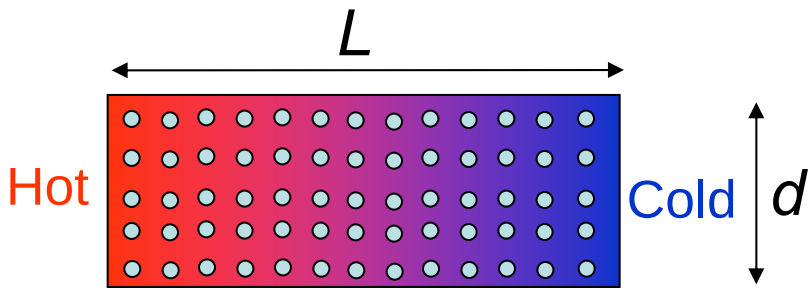

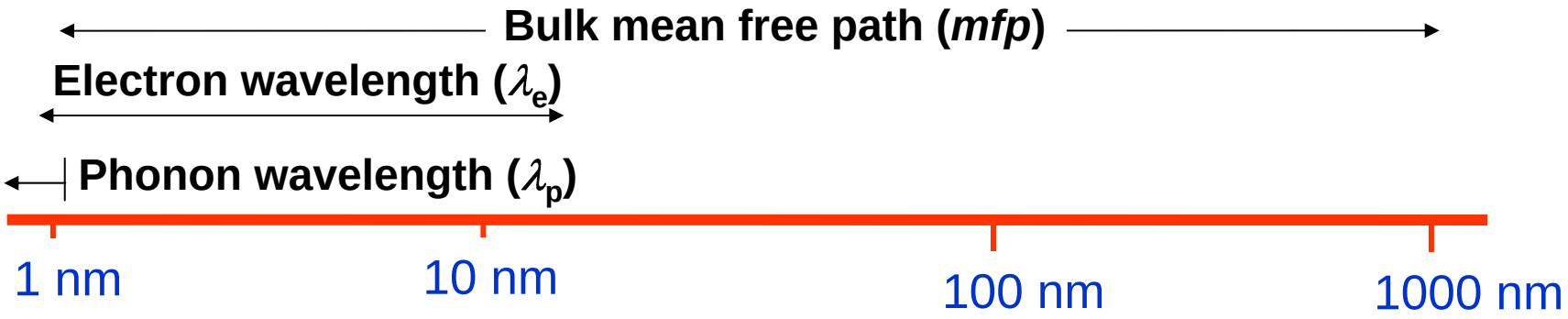

- d ~ bulk *mfp* → classical size effects: modified *mfp*
- d ~ wavelength (λ) → quantum size effects: modified density of states, increased electron-electron interaction

Quantum Wells and Wires

- Although $\overline{E}_{1D} > \overline{E}_{2D} > \overline{E}_{3D}$, the same carrier concentration n can be obtained.

- $|S| \approx (\overline{E} - E_F)/eT$, so that

  $|S_{1D}| > |S_{2D}| > |S_{3D}|$

  when $n_{1D} = n_{2D} = n_{3D}$

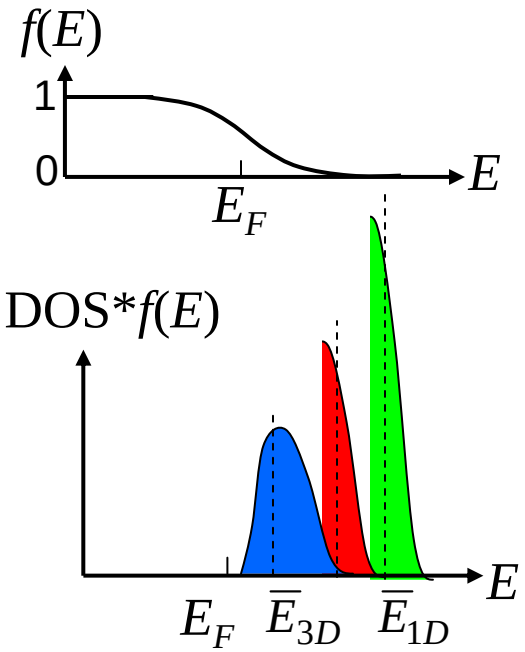

$$ZT \equiv \frac{S^2\sigma}{\kappa}T \uparrow$$

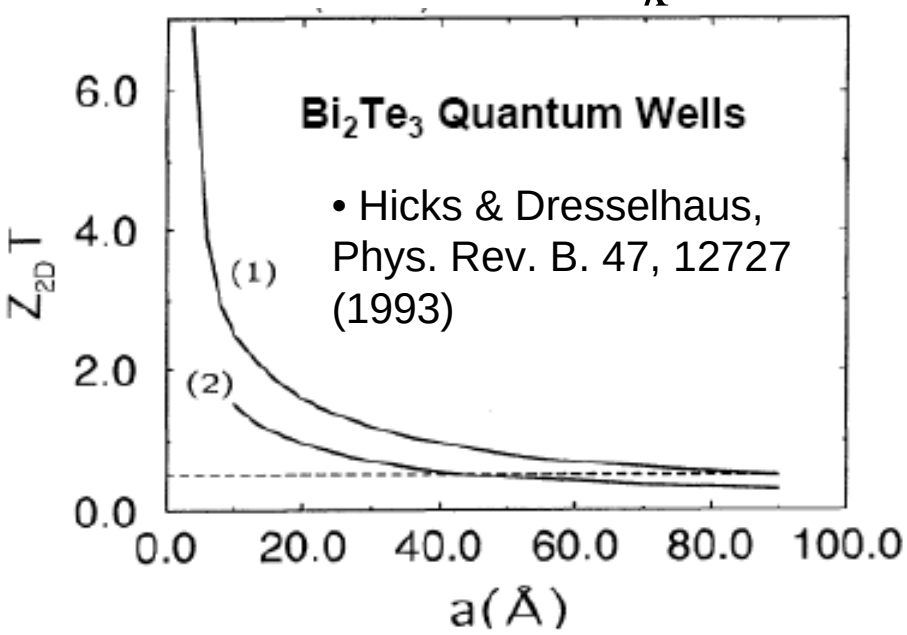

Nanostructured Thermoelectric Materials

•Quantum well superlattices

•**Venkatasubramanian et al. *Nature* 413, 597 (2001)**

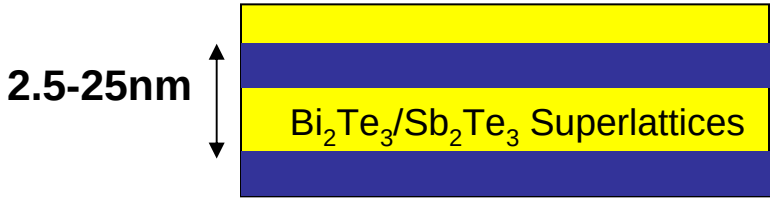

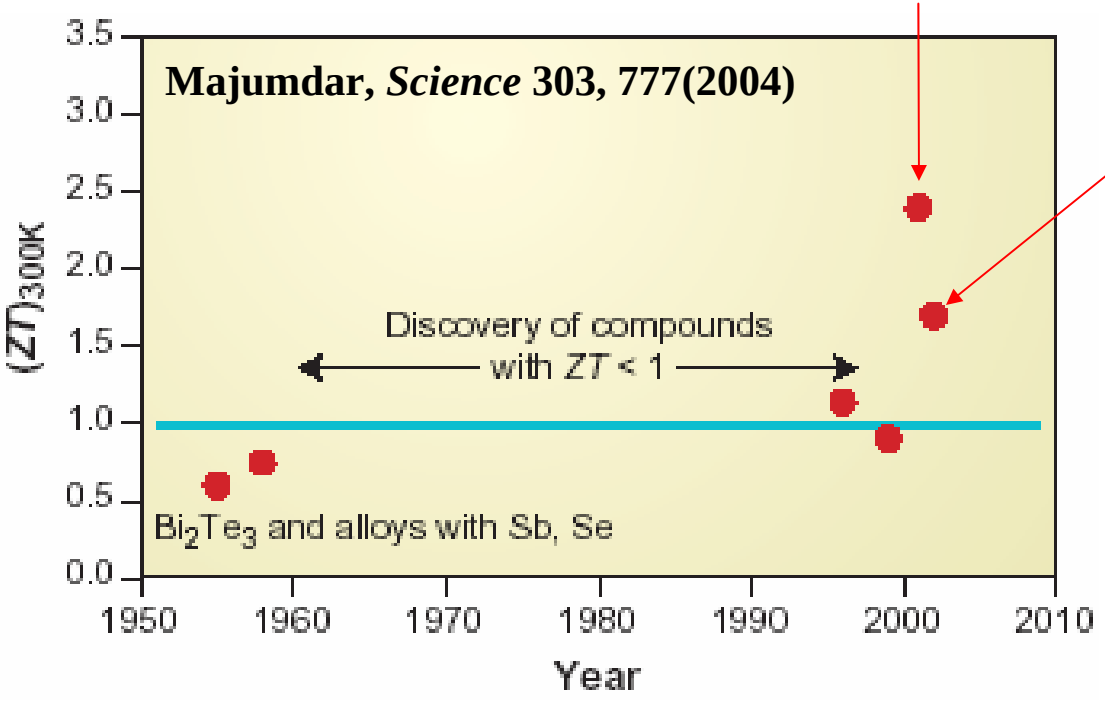

The *ZT* improvements were attributed to κ reduction from phonon boundary scattering, instead of $S^2\sigma$ increase from quantum confinement of electrons.

•Quantum dot superlattices

Harman et al., *Science* 297, 2229 (2002)

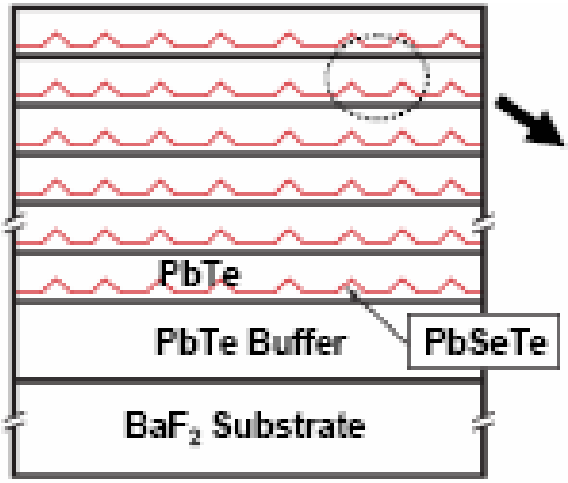

•Nanostructured bulk thermoelectric materials

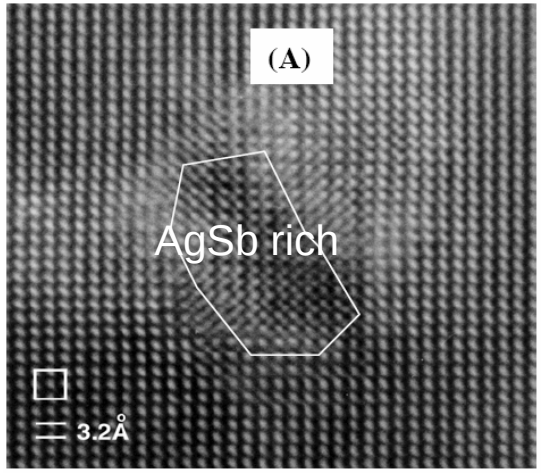

$AgPb_{18}SbTe_{20}$
$ZT \approx 2$ @ 800K

Hsu et al., *Science* 303, 818 (2004)

Phonon-boundary Scattering

- Phonons: lattice vibration waves

TEM of a thin film superlattice

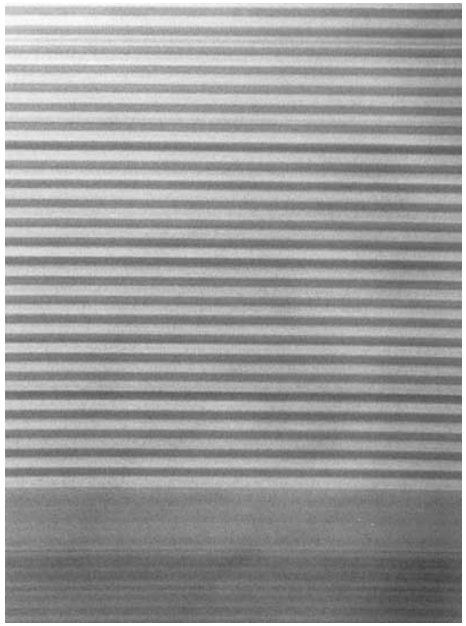

Specular scattering

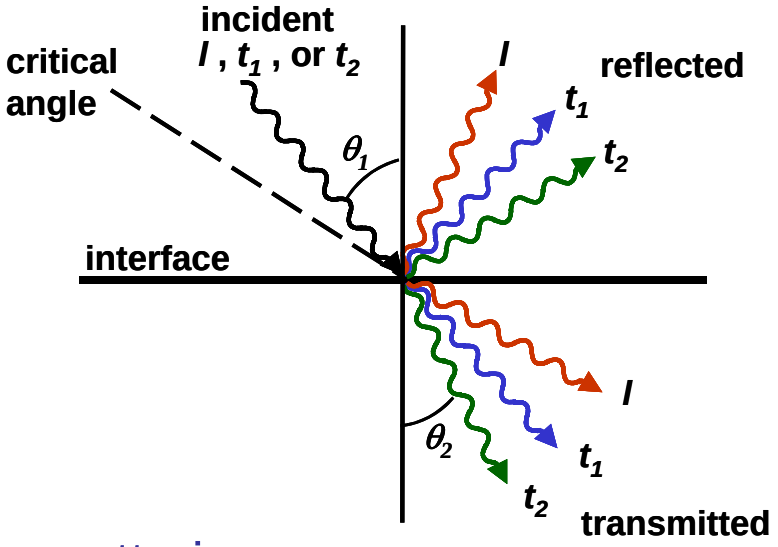

Diffuse scattering

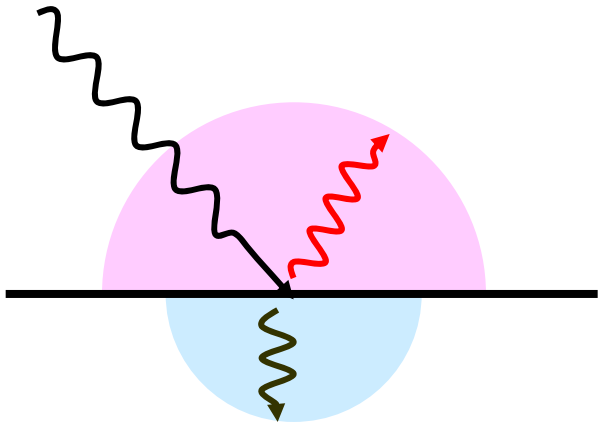

Courtesy of A. Majumdar

Outline

- Thermoelectrics of bulk and nanostructured materials

➢ Probing local thermopower of quantum wells

- Thermoelectric characterizations of individual nanowires using nanofabricated devices

- Integration of metal oxide nanowires with microsystems for nerve agent detection

UHV Scanning Thermoelectric Microscopy (SThEM)

- **Objective:**
  - **To verify *S* enhancement in quantum wells**

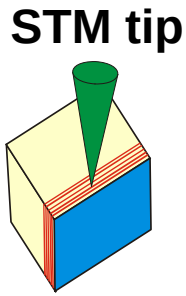

STM ⟷ SThEM

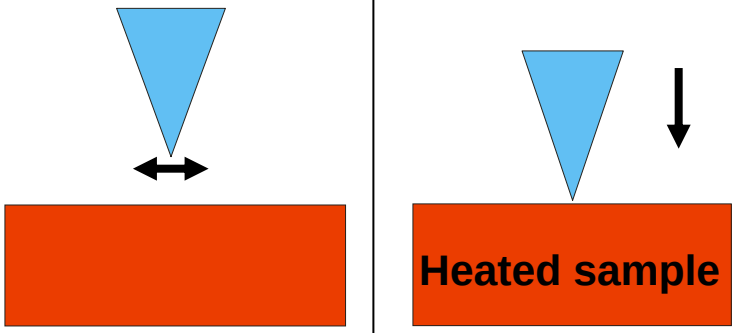

- Apply a voltage
- Regulate the tip-sample gap to maintain a constant tunneling current

- Disable STM feedback control
- Zero STM bias
- Connect tip & sample to an electrometer
- Move STM tip toward the sample

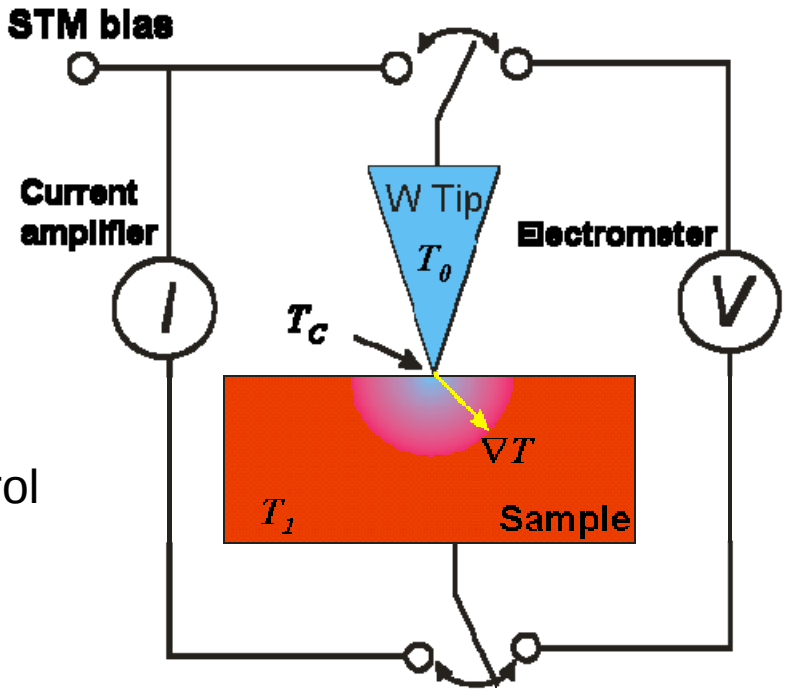

$S_{\text{semic sample}} >> S_{\text{tip}} \rightarrow$

$$V \approx S(x,y)(T_1 - T_C)$$

Model System: p-n Junctions

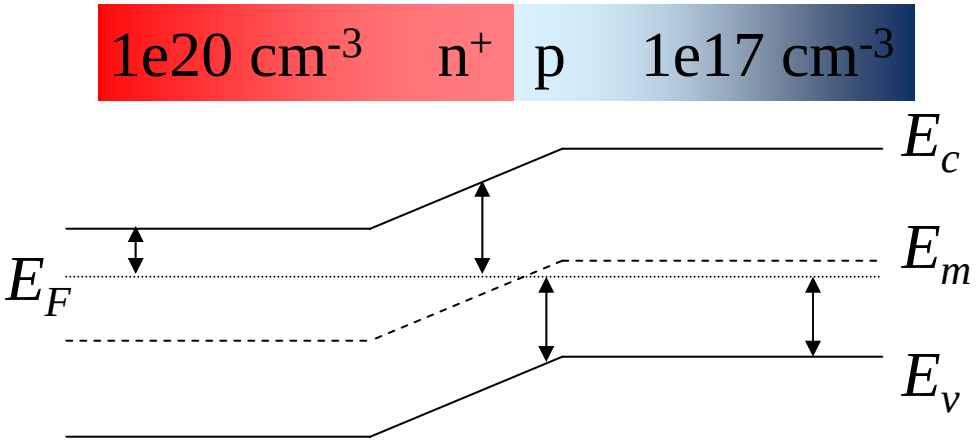

$$S = \frac{n\mu_e S_e + p\mu_h S_h}{n\mu_e + p\mu_h}$$

n-doped

$$S \approx S_e = \frac{1}{-eT}(E_c - E_F + \frac{3}{2}k_B T) < 0$$

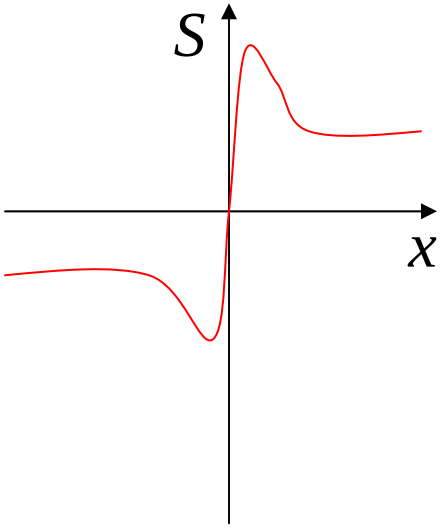

p-doped

$$S \approx S_h = \frac{1}{eT}(E_F - E_v + \frac{3}{2}k_B T) > 0$$

Thermoelectric Profiling of p-n Junctions

STM image of a GaAs p-n junction

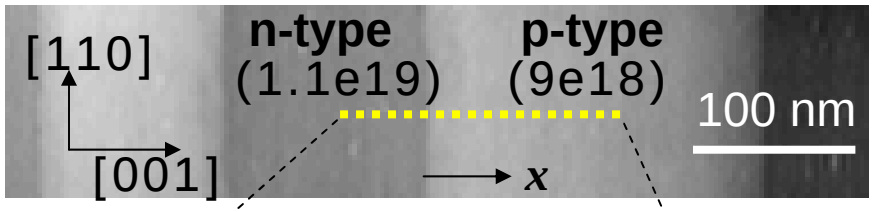

N (cm^{-3})	d_{dopant} (nm)	Resolution (nm)
1e19	4.6	8
1e18	10	20

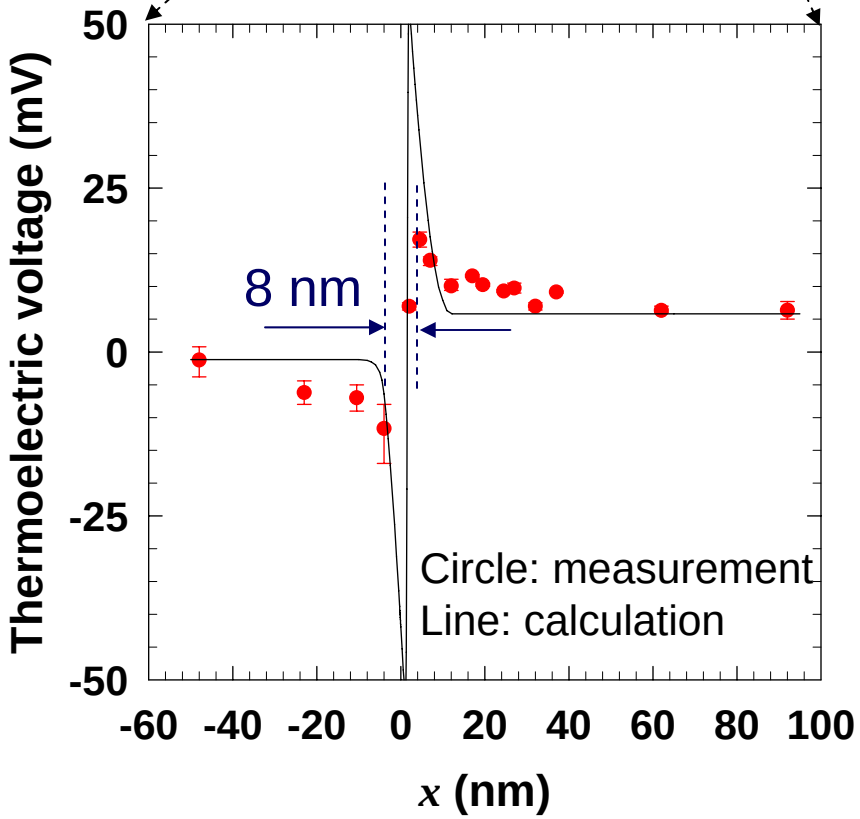

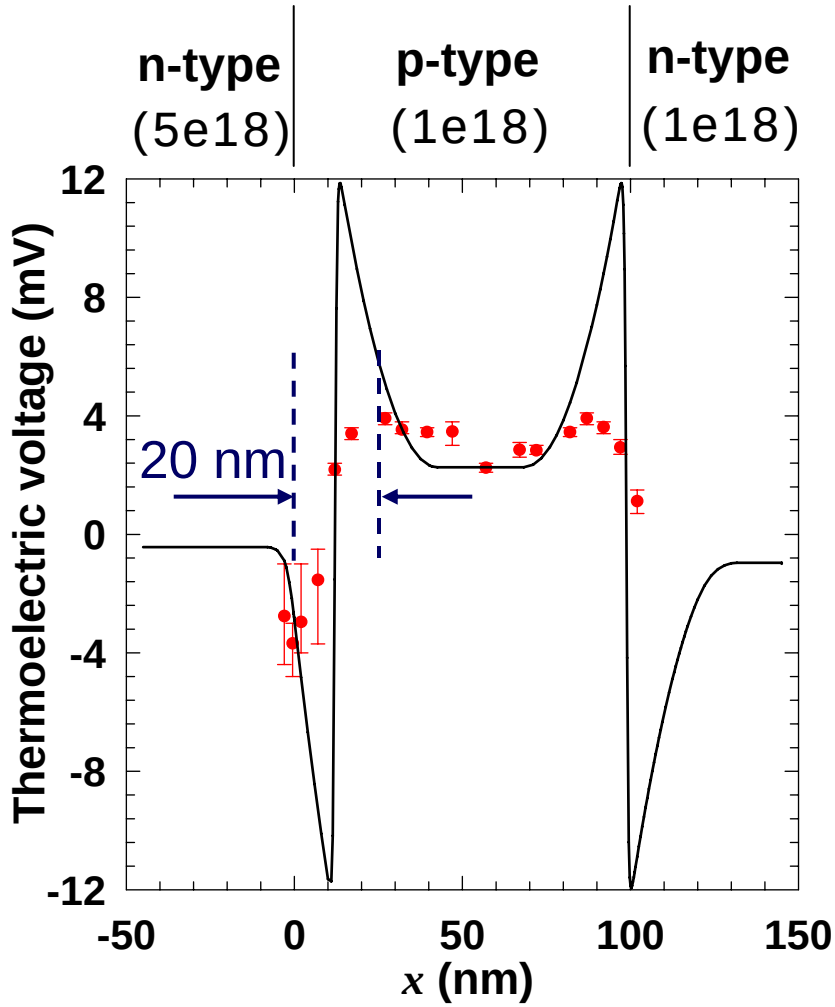

Lyeo, Khajetoorians, Shi, Pipe, Ram, Shakouri, Shih, *Science* 303, 816 (2004)

Seebeck Enhancement in Quantum Wells

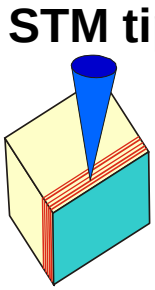

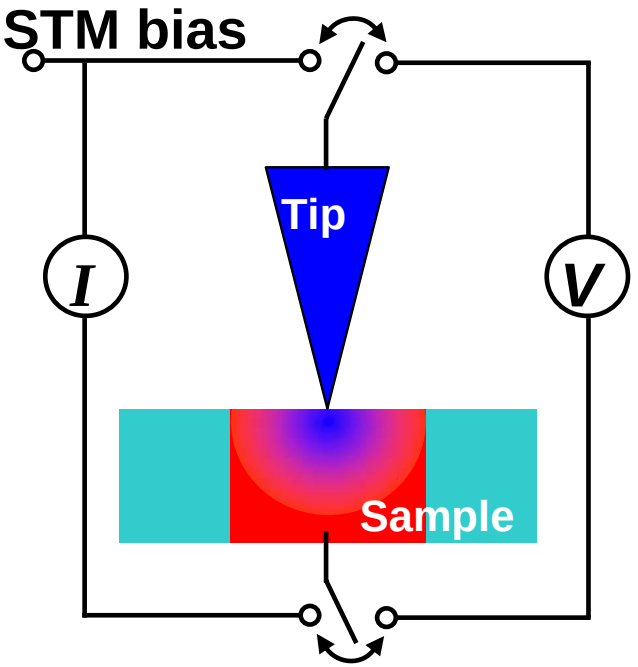

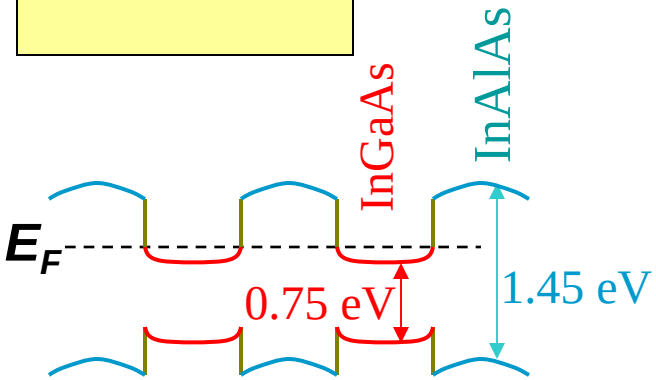

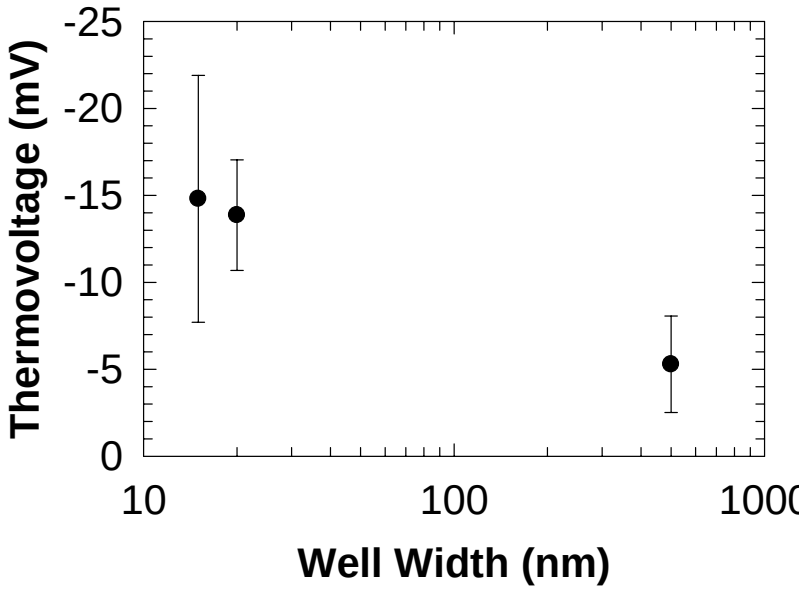

Collaboration: Shakouri Group & Gossard Group

Outline

- Thermoelectrics of bulk and nanostructured materials
- Probing local thermopower of quantum wells
- ➢ Thermoelectric characterizations of individual nanowires using nanofabricated devices
- Integration of metal oxide nanowires with microsystems for nerve agent detection

Thermoelectric Transport in Nanowires

- Figure of Merit (ZT)

$$ZT \equiv \frac{S^2\sigma}{\kappa}T$$

- Lin et al., PRB 62, 4610 (2001)

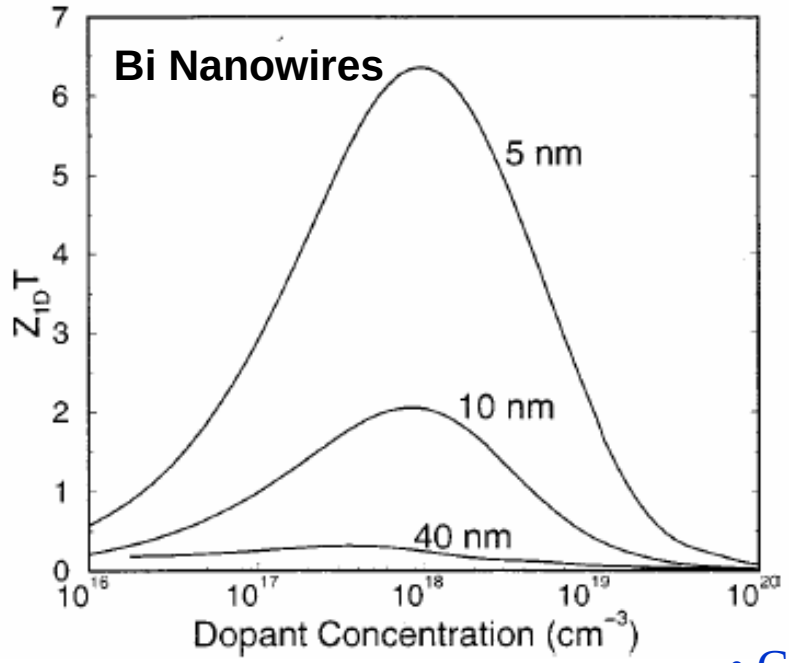

- $S^2\sigma$ increases due to asymmetric DOS (Hicks & Dresselhaus, 1993)
- Diffuse phonon- surface scattering → suppressed κ

- Mingo, APL 88, 149902 (E) (2006)

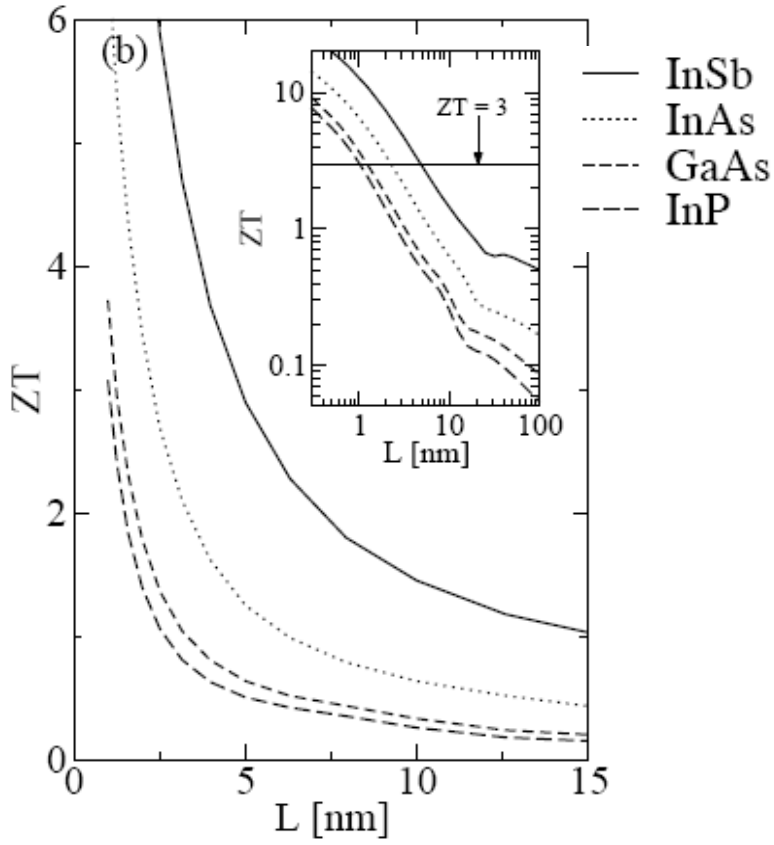

- Conditions & Assumptions:
  - Single crystal
  - Doping concentration optimized for maximum $S^2\sigma$
  - Surface is diffuse for phonons and specular for electrons
  - Electron-electron interaction ignored

InSb

- **Bulk Pure InSb**:

  ZT = 0.6 at T = 673 K (Yamaguchi et al., APL **87**, 201902 (2005))

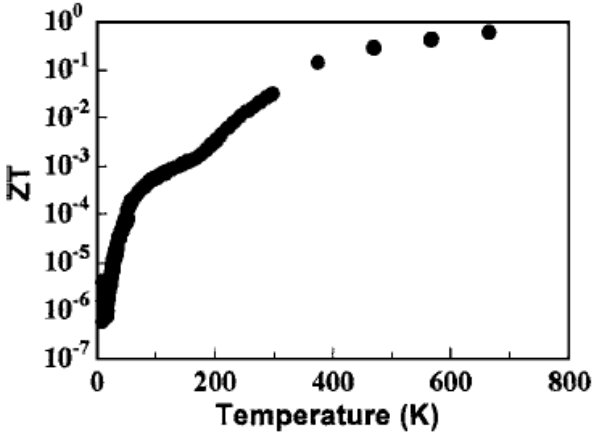

- **InSb Nanowires:**

  Largest ZT enhancement predicted among III-V nanowires (Mingo, APL 88, 149902 (E) (2006))

- **VLS (vapor-liquid-solid) InSb Nanowires (Ye & Mingo, NASA Ames)**

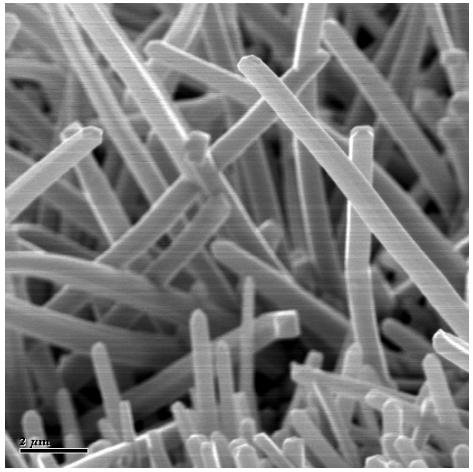

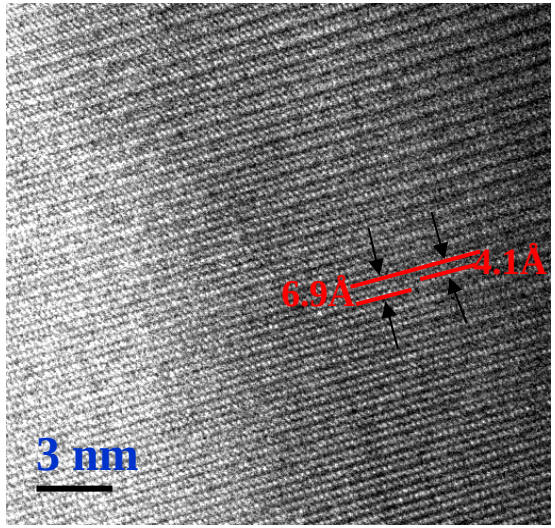

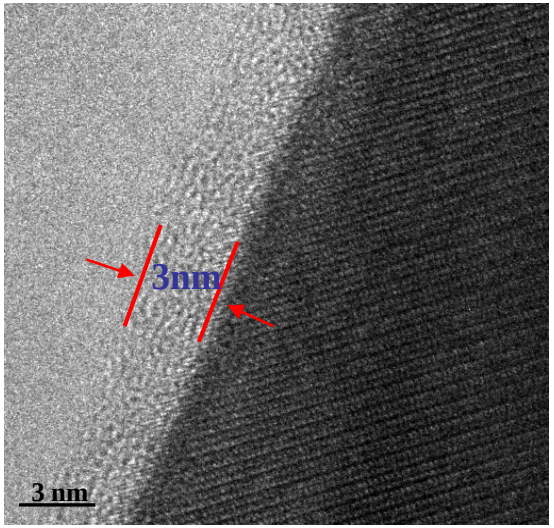

- Single crystal
- Growth direction [001]
- Surface roughness 0.5-1 nm

Seebeck Coefficient of an InSb Nanowire

- Au/Cr electrodes were patterned using EBL and lift-off on the nanowire.
- The nanowire surface at the contact areas were passivated using $(NH_4)_2S$.

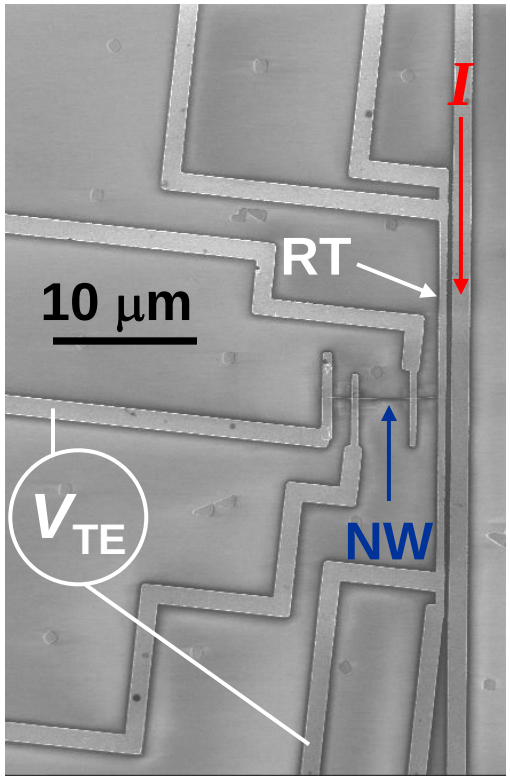

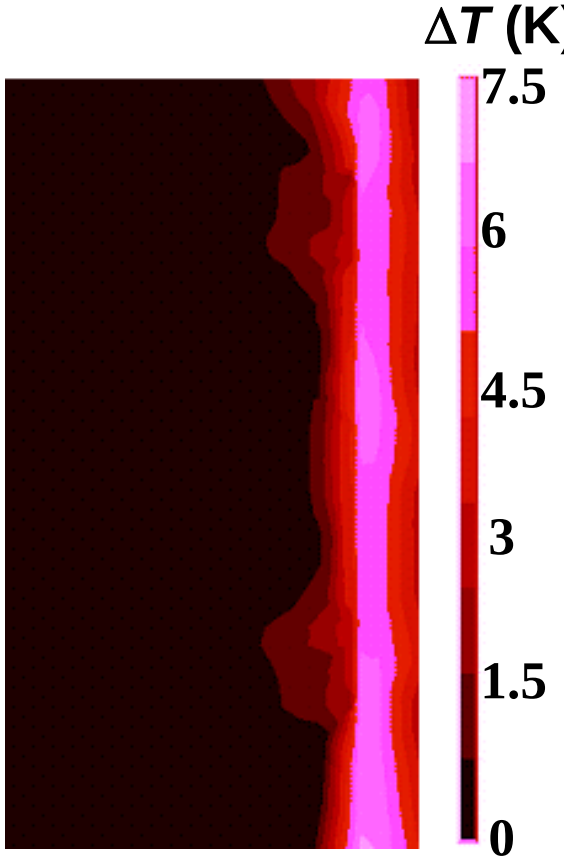

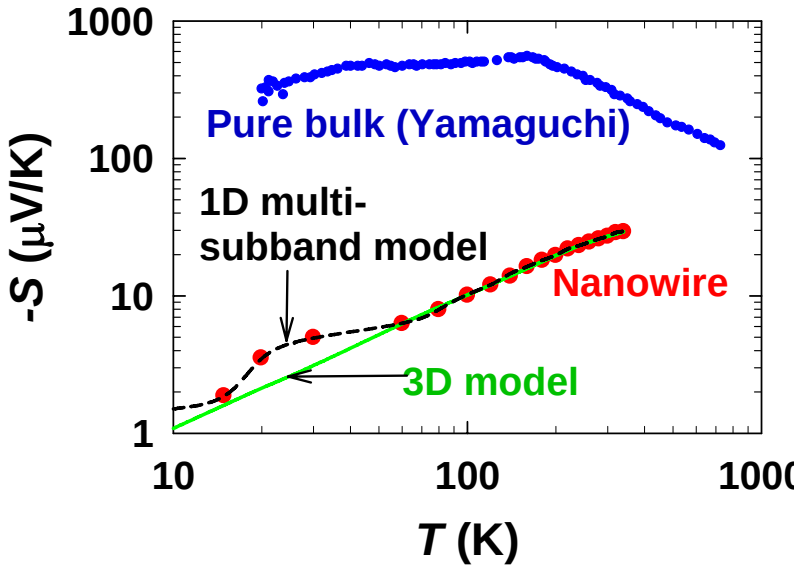

$$S = V_{TE}/\Delta T$$

$$S = \frac{1}{eT}\left((E_F - E_C) - \frac{\int_0^\infty g(E)\tau_e E^2 \frac{\partial f_0(E)}{\partial E} dE}{\int_0^\infty g(E)\tau_e E \frac{\partial f_0(E)}{\partial E} dE} \right)$$

- Diameter d = 42 nm, subband separation:

$$\Delta E \approx \left(\pi^2\hbar^2\right)\Big/ m_e^* d^2 \sim k_B T \text{ at } T \approx 300K$$

J. H. Seol, Arden Moore et al.

Electrical Conductivity

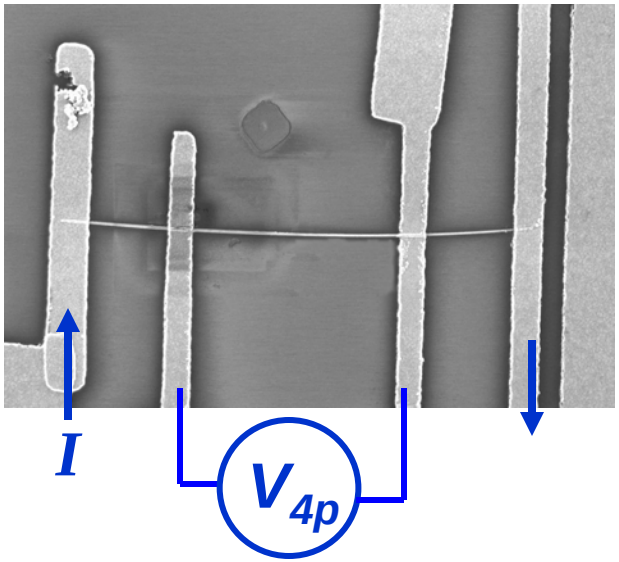

$$\sigma = ne\mu$$

- Carrier concentration: $n(T) = \int_0^\infty g(E)\, f_0(E) dE$
- Mobility: $\mu^{-1} = \mu_{bulk}^{-1}(n, T) + \mu_{boundary}^{-1}$
- Boundary scattering mean free path: $L_B \approx 52$ nm $\sim d$
- Roughness r ~0.5-1 nm, Fermi wavelength λ_F~ 20 nm, surface specularity for electrons:

$$p(\lambda) \approx \exp(-16\pi^3 r^2 / \lambda^2) \approx 0.26 - 0.73$$

→ partially diffuse, partially specular

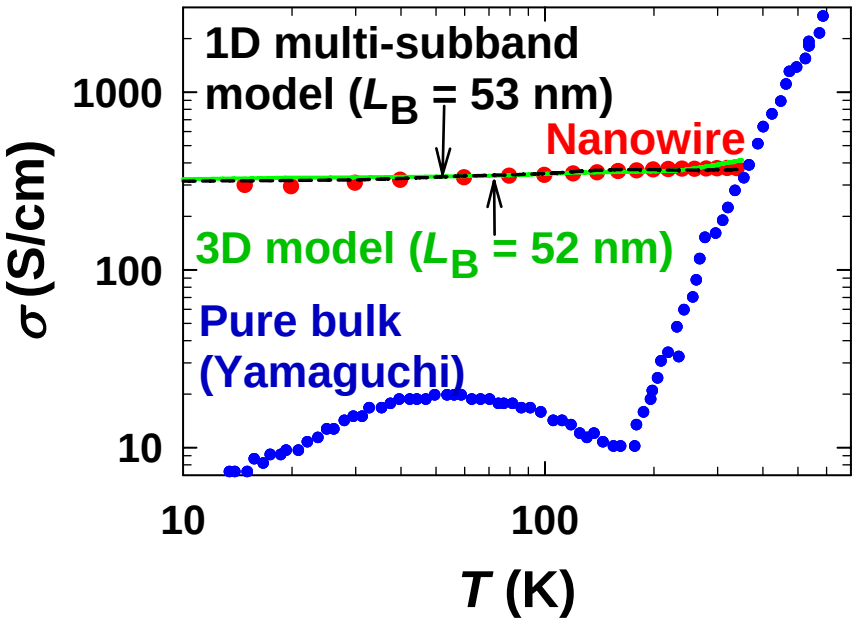

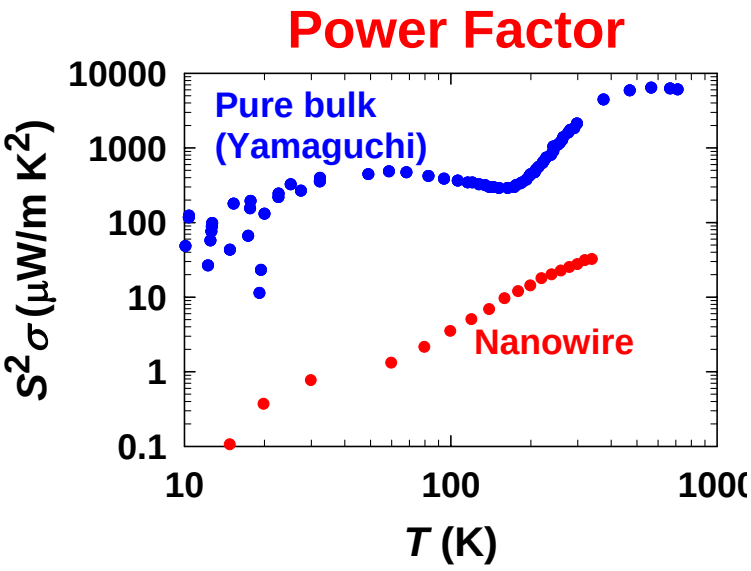

Fermi Level (E_F)

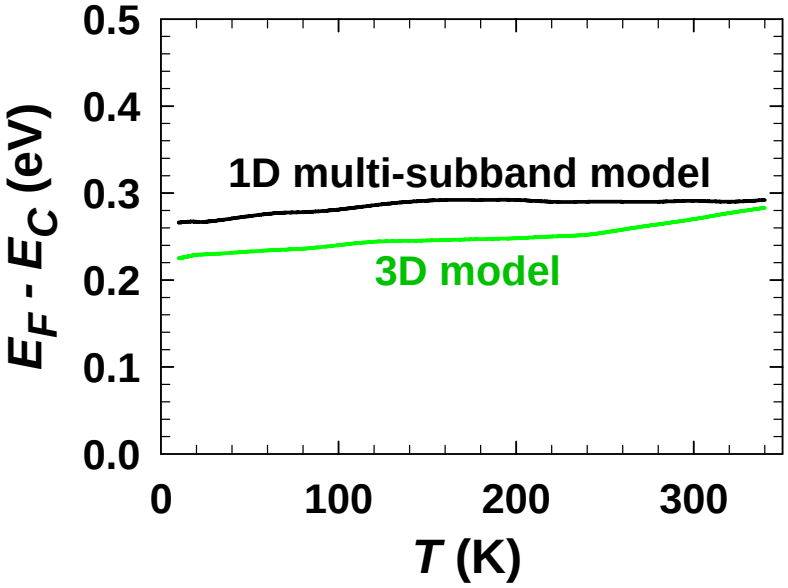

• Carrier Concentration

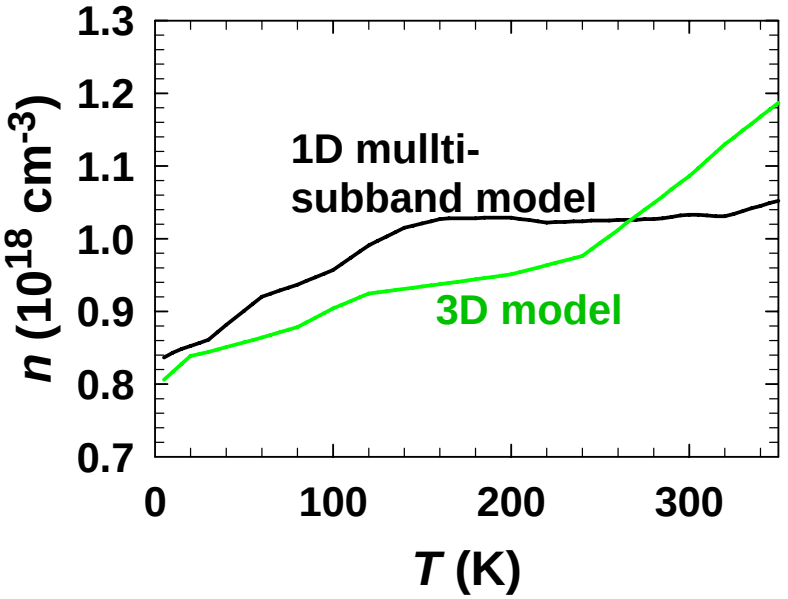

• E_F lies in the 8th electron subband.

• Carrier concentration >> intrinsic n ~ 2 x 10^{16} cm^{-3} at 300 K

• Highly degenerately doped, possibly with Te → low power factor

• E_F and S can be tuned by controlling the doping or using a gate voltage.

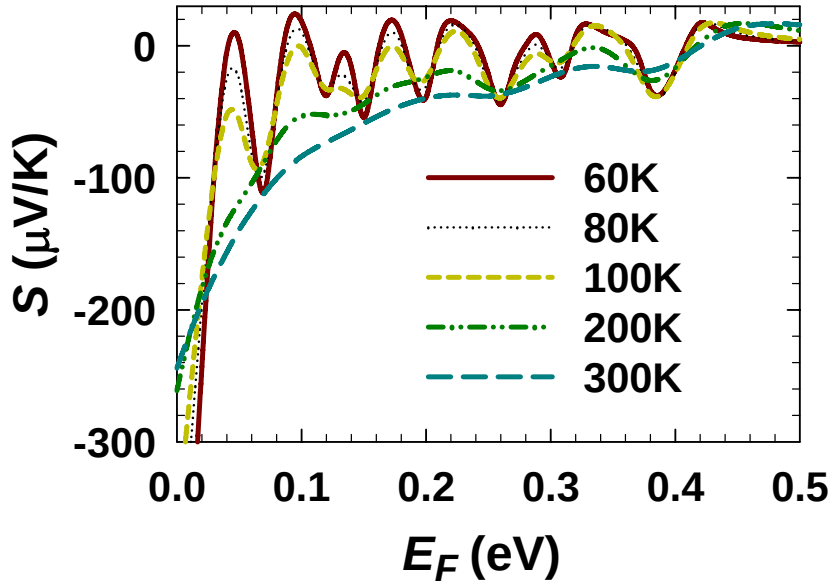

Combined TE & TEM Characterizations of the Same Nanowire

- Microfabricated devices for measuring TE properties (σ, κ, S, ZT), TEM, EDS of the same nanowire or suspended thin film

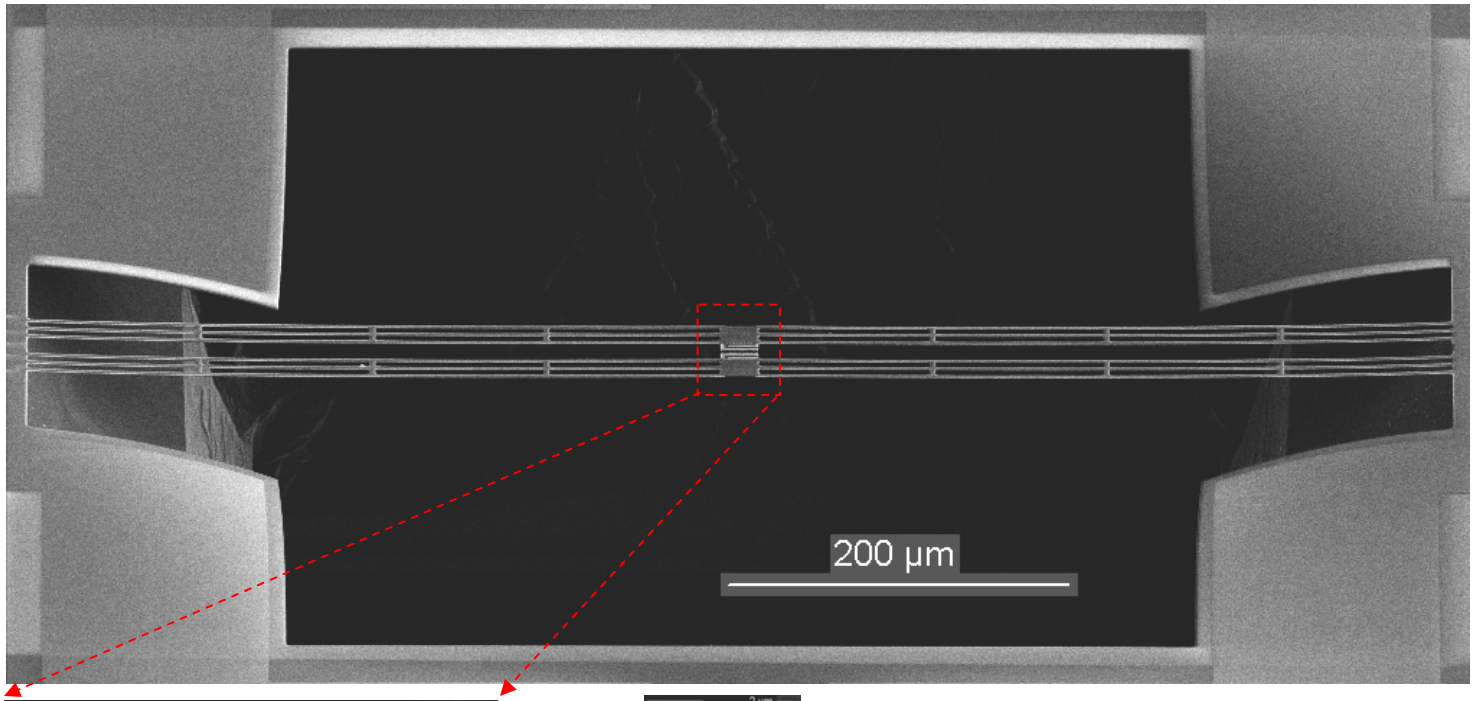

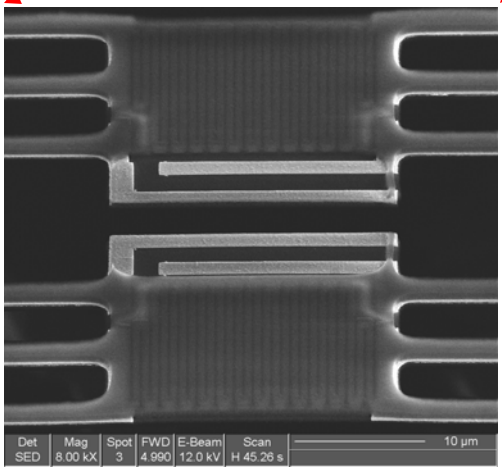

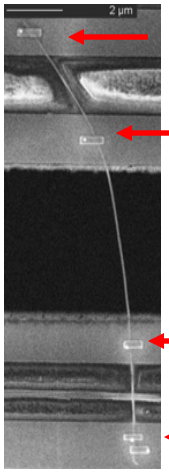

Electrical contact to the nanowire made possible by Electron Beam Induced Metal Deposition (EBIMD) or Ion Beam Induced Metal Deposition (IBIMD)

Electrodeposited $Bi_{1-x}Te_x$ Nanowires

- Bi_xTe_{1-x} nanowire arrays electrodeposited in nanopores of anodized alumina templates (AAMs) by W. Wang, Q. Jin, and Prof. X. G. Li at USTC

  -- Crystalline structure

  -- Growth direction $[11\bar{2}0]$, perpendicular to C axis

  -- The atomic ratio (x) was varied by changing the ratio in the electrolytes

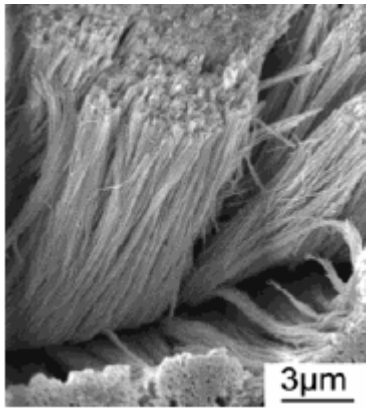

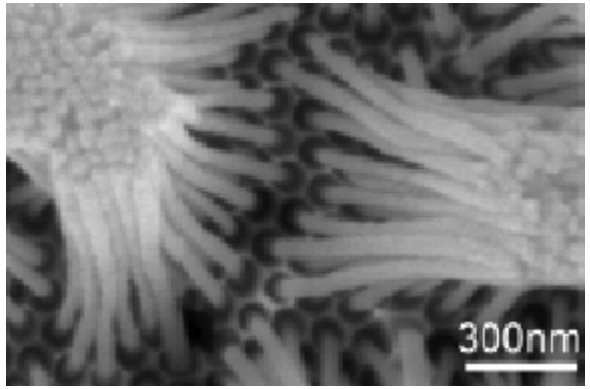

X. G. Li group, *J. Phys. Chem. B* **2004**, *108*, 1844

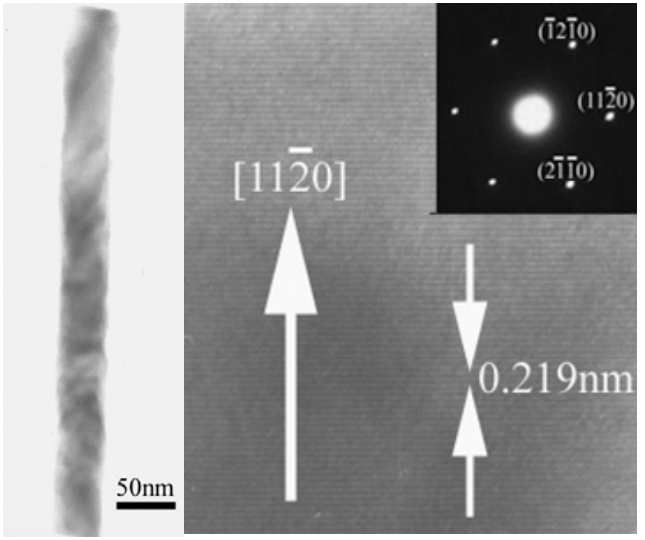

Seebeck Coefficient of $Bi_{1-x}Te_x$ Nanowires

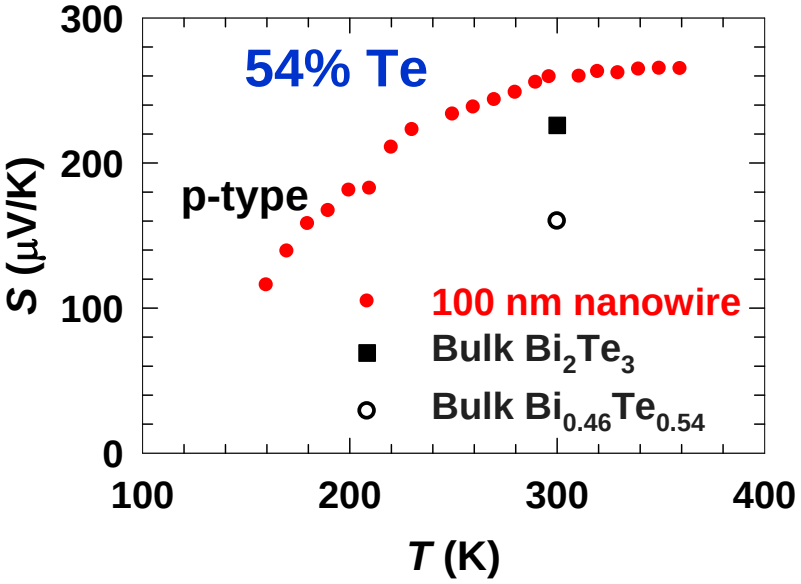

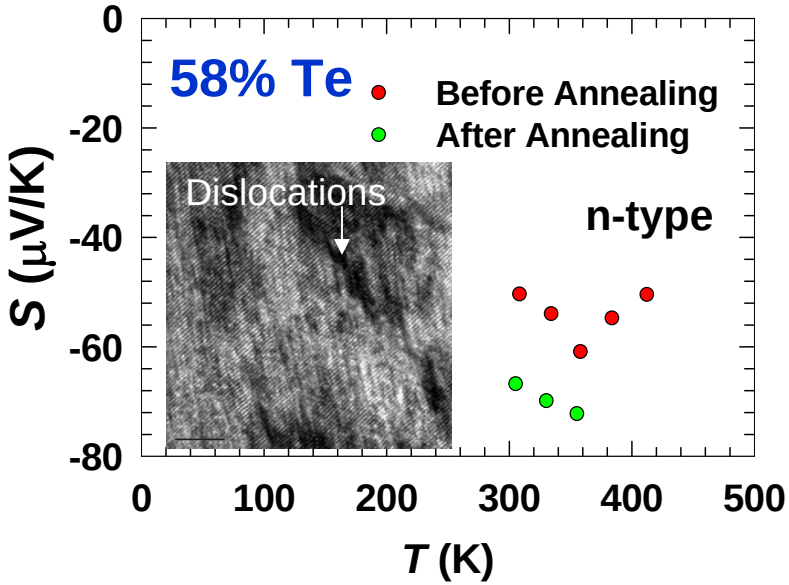

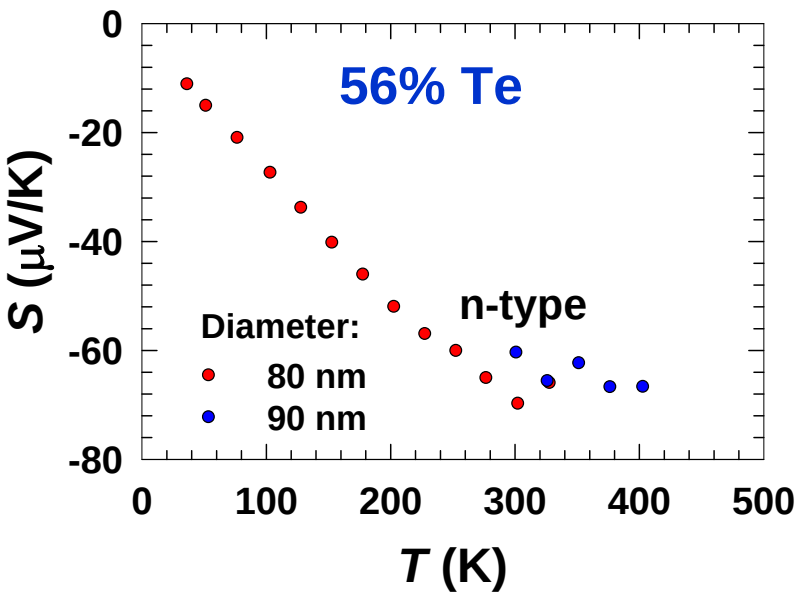

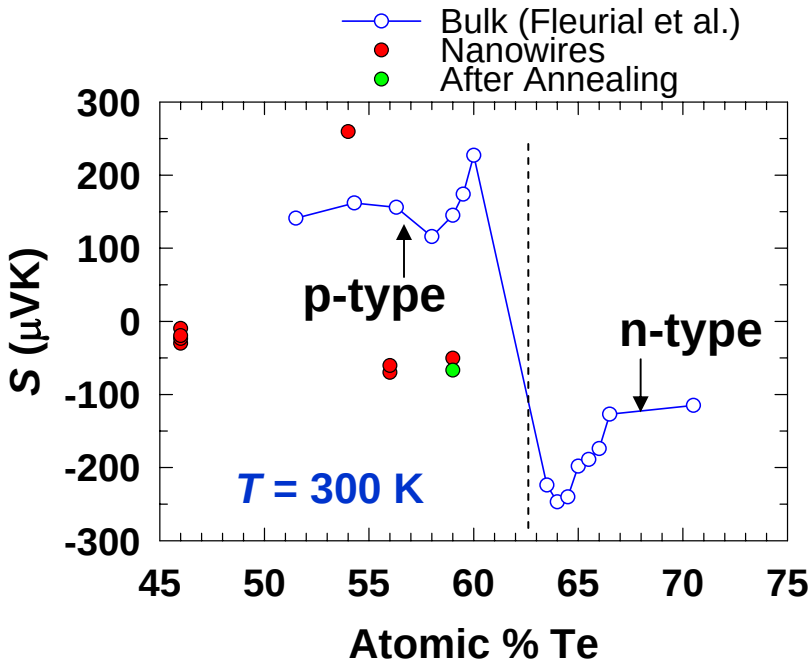

$ZT \equiv S^2\sigma T/\kappa$ of $Bi_{1-x}Te_x$ Nanowires

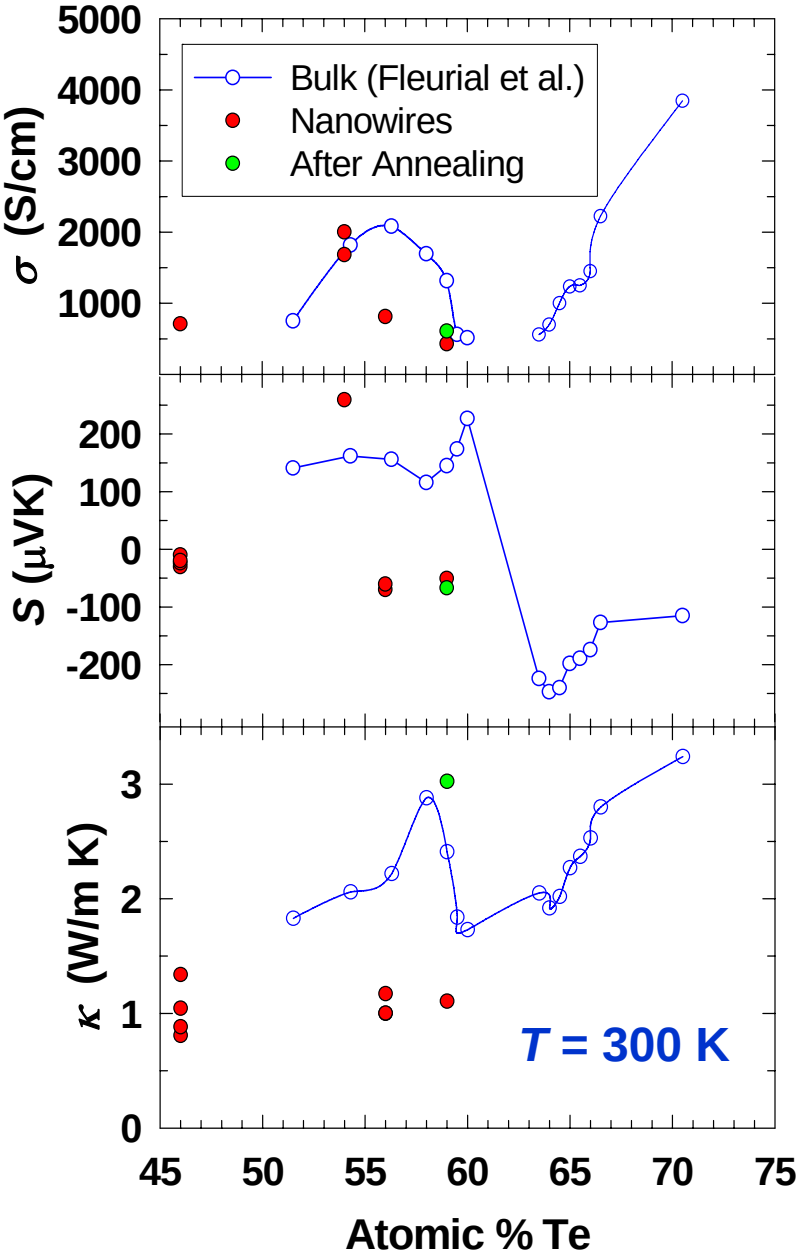

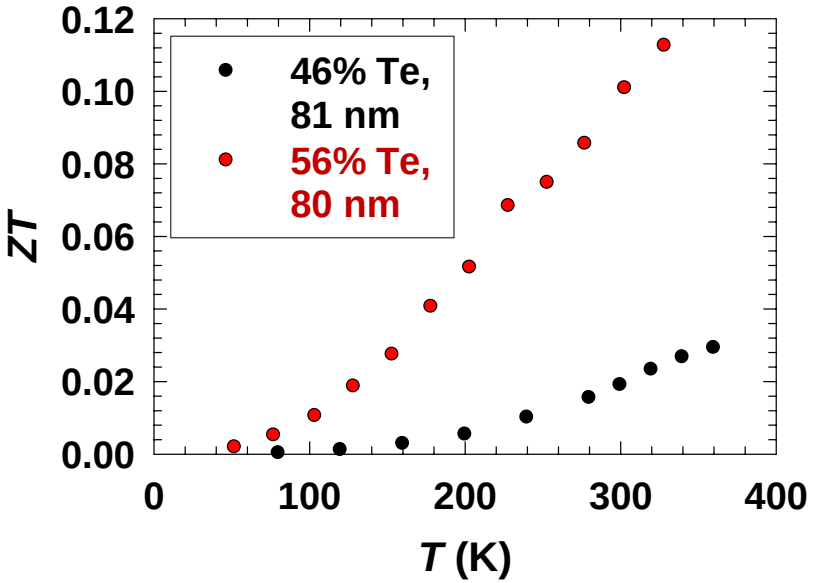

- The κ and ZT of the 54% Te sample were not obtained.

- The 54% Te sample has higher σ, indicating fewer dislocations/defects, which could have resulted in the larger S and potentially lead to much higher ZT than the 46% Te and 56% Te samples.

Lessons Learned

- Quantum confinement of electrons can lead to Seebeck improvement in quantum wells with sharp interfaces.

- The observed low to modest power factors of $Bi_{1-x}Te_x$, III-V, and silicide nanowires are attributed to dislocations/defects, impurities (e.g. oxygen), partially diffuse surface scattering, and surface states.

Outline

- Thermoelectrics of bulk and nanostructured materials
- Probing local thermopower of quantum wells
- Thermoelectric characterizations of individual nanowires using nanofabricated devices

➢ Integration of metal oxide nanowires with microsystems for nerve agent detection

Metal Oxide Sensors

- Commonly used for monitoring toxic and inflammable gases
- The sensing mechanism is based on surface reduction-oxidation (redox) processes

→Changing the concentration of oxygen vacancies and thus the electrical conductance

e.g. NO_2 (gas) + e^- → NO_2^- (surface) : Reduces conductivity

CO (gas) + O^- (surface) → CO_2 (gas) +e^- : Increases conductivity

- Redox processes can be enhanced at high temperatures to increase the sensitivity

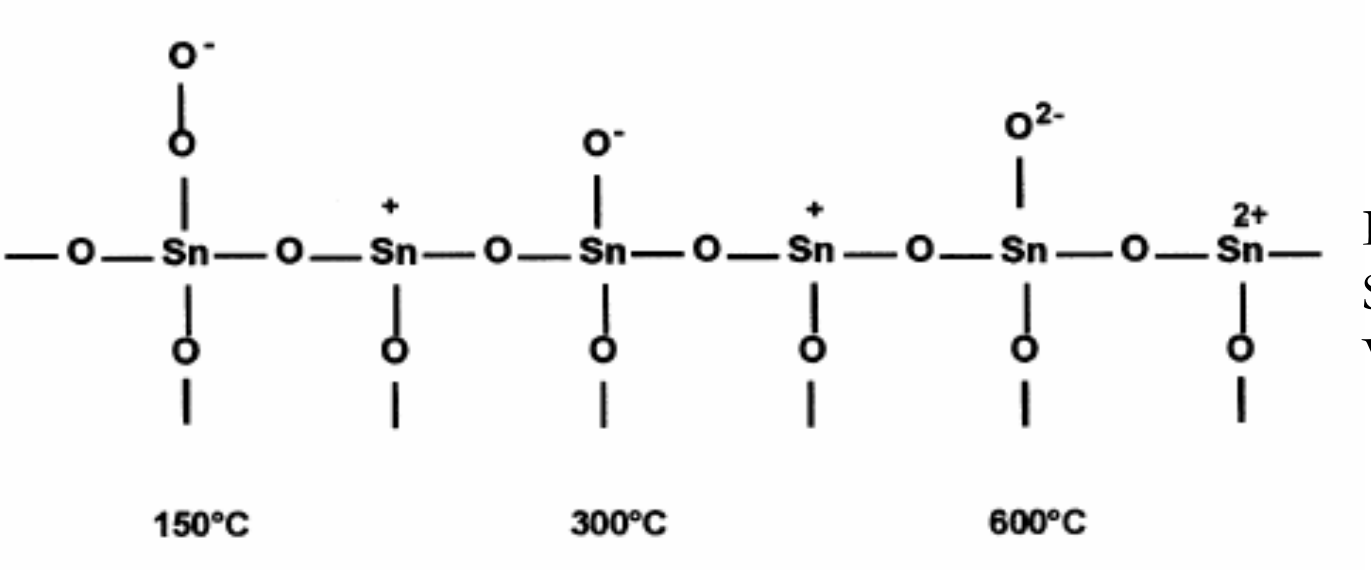

Ruhland *et al.* (1998) Sens. Actuat. B Vol.50, pp. 85~94

Thin Film Metal Oxide MEMS Sensors

Chan et al., Sens. Actuat. B 46, 174 (1998)

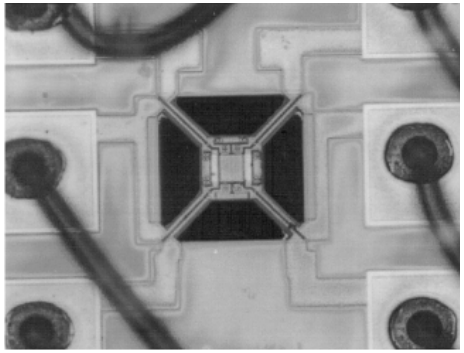

Lee *et al.*, Sens. Actuat. B, 67, 122 (2000)

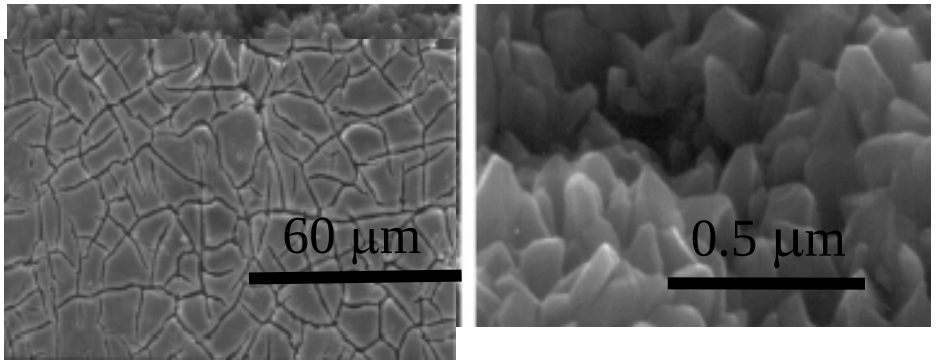

- Sensor temperature can be controlled by a low-power suspended MEMS (microelectromechanical systems) heater
- The surface redox processes modulate electron transport only in the surface depletion region (~ the Debye electrostatic screening length) → limited sensitivity
- Grain boundaries → sensor poisoning & lack of repeatability and stability
- High density of pinholes and defects → unstable electrical properties

Benefits & Problems of Metal Oxide Nanowire Sensors

• Single-crystal SnO_2 nanobelts grown by the vapor-solid method (Z.L. Wang Group)

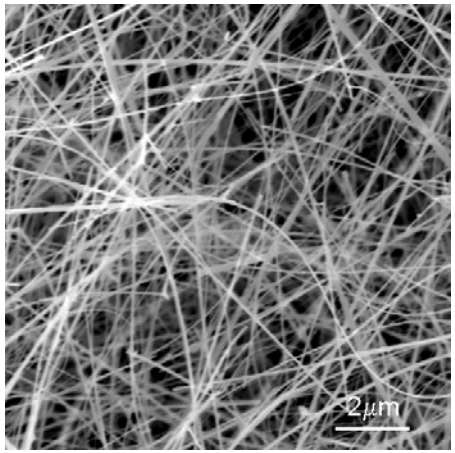

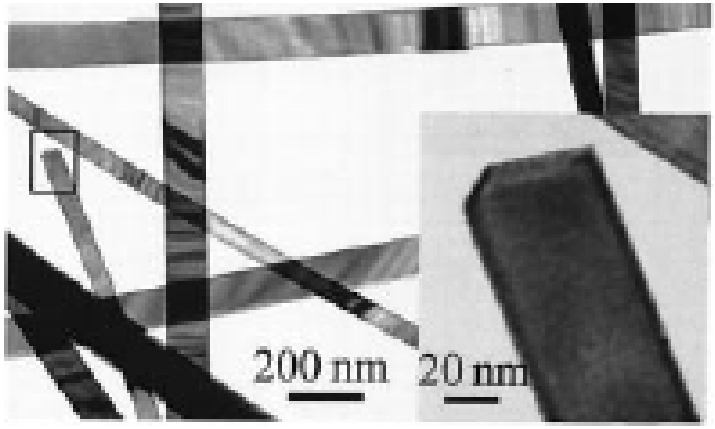

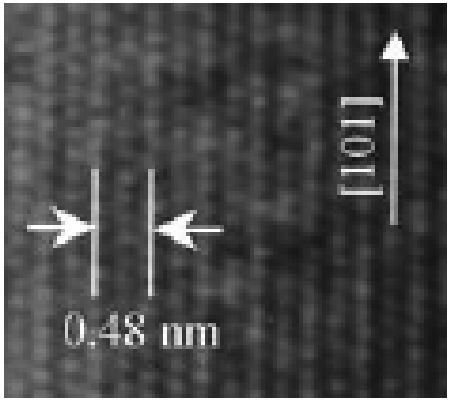

• Potential Benefits:

-Single-crystal structure → Eliminating grain boundary poisoning → Stable & reproducible?

-Thickness ~ 10-50 nm, approaching the Debye length → High sensitivity?

• Problems:

-Making Ohmic contacts to metal oxide nanowires

-Sensor response can saturate when the gas concentration is higher than a certain value → small dynamic range?

-Wafer-scale fabrication of sensor devices containing metal oxide nanowire sensing elements

Integration of Metal Oxide Nanowires with Microsystems

C. Yu, Q. Hao, L. Shi, X. Kong, Z. L. Wang, 2005, Appl. Phys. Lett. 86, 063101+Cover

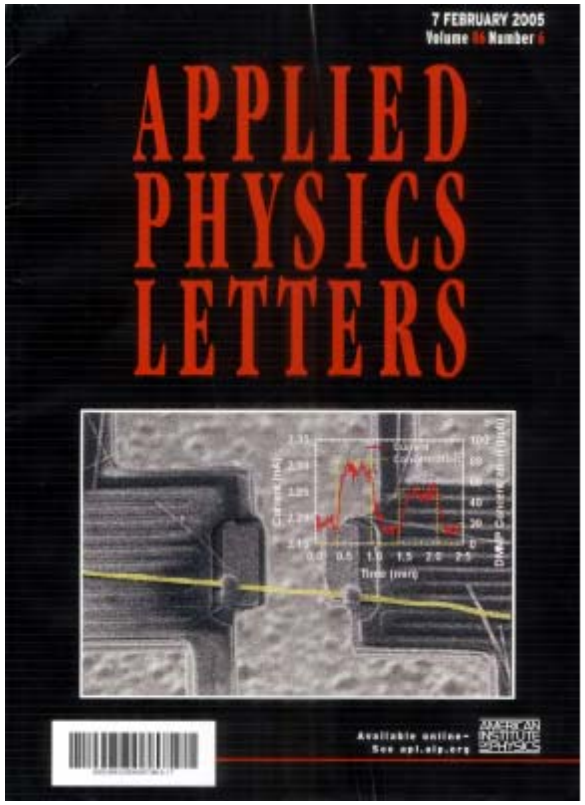

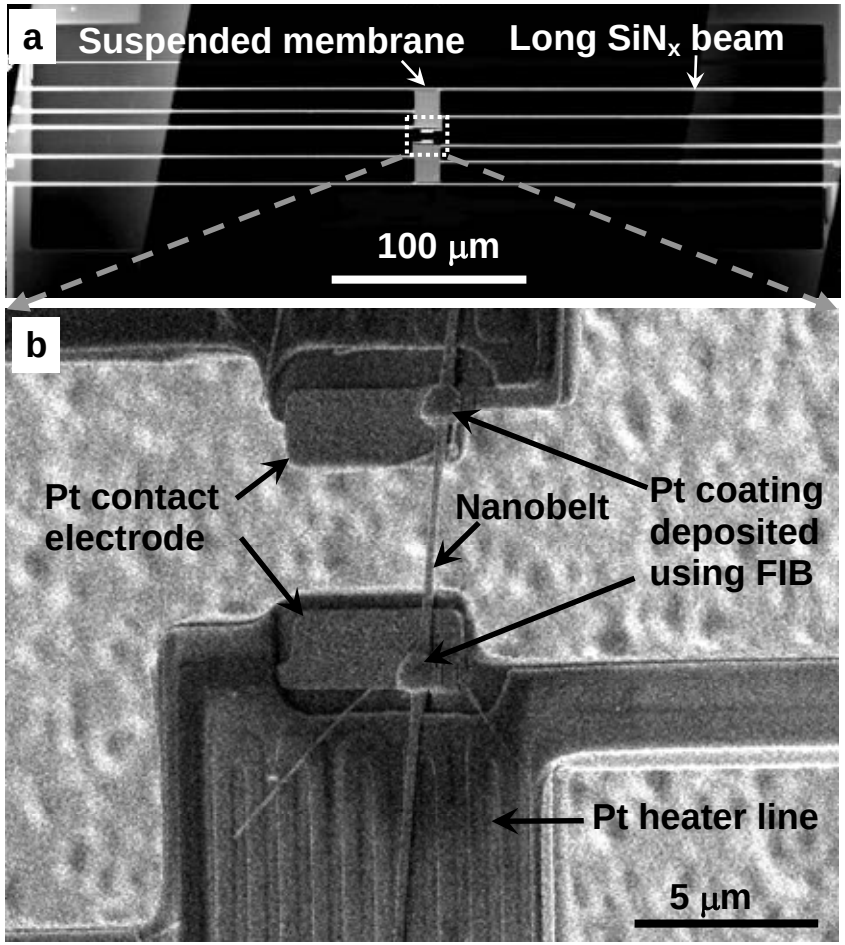

- Dielectrophoresis assembly of nanowires with microsystems

Response of a SnO_2 Nanobelt-MEMS Sensor to NO_2

Power consumption

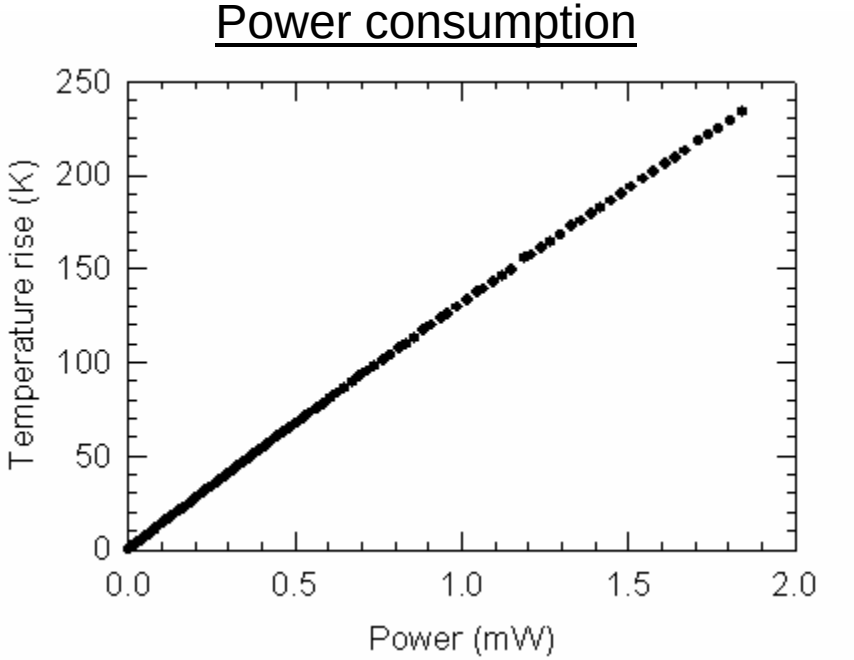

Response to NO_2 in air

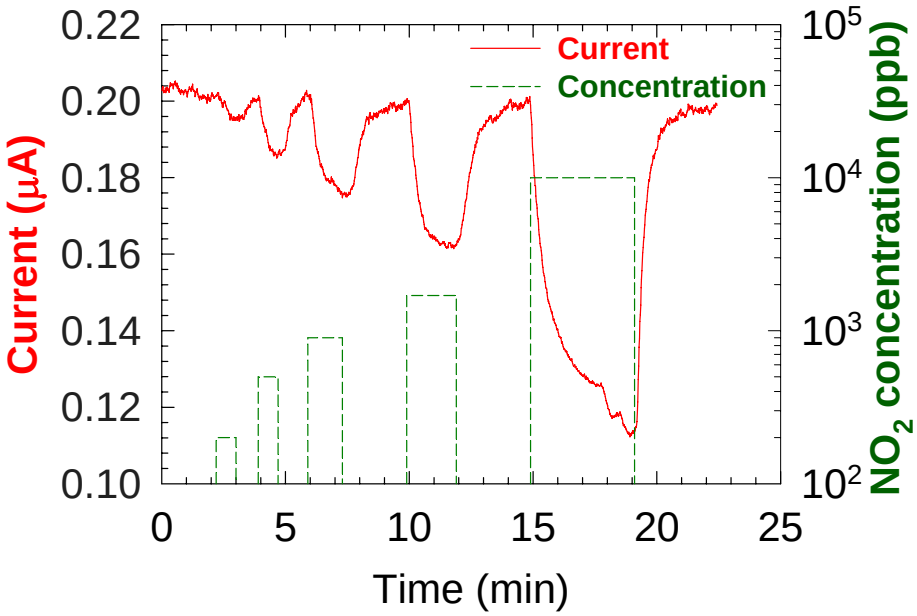

- The sensor was heated to 200°C using the low-power MEMS heater
- Full recovery upon purging the sensor with room air, no grain boundary poisoning
- Sensitivity ~ 100 ppb

Interaction of Nerve Agents with Metal Oxides

•Organophosphorous compounds are strong inhibitors for the enzymes for nerve functions and can be used as insecticides and nerve agents.

•Dimethyl methylphosphonate (DMMP) is a benign simulant to nerve agents

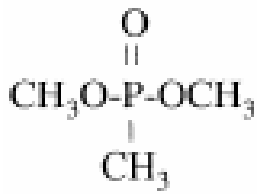

Kim et al., "Interaction of organophosphorous compounds with TiO_2 and WO_3 surfaces probed by vibrational spectroscopy," Sensors &Actuators B 76, 442 (2001):

• It was found that room temperature adsorption of DMMP was through H-bonding of the P=O group to the OH group on the metal oxide

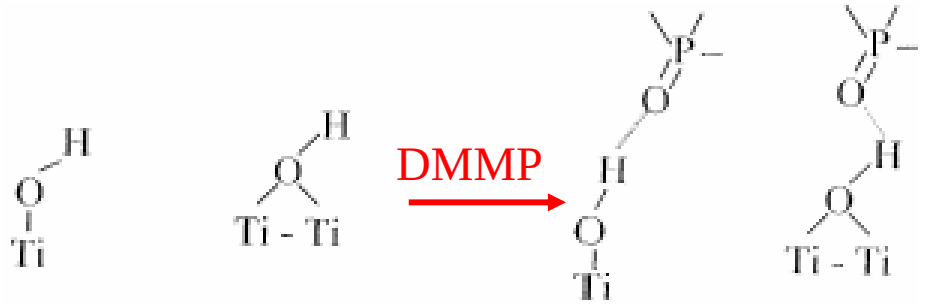

Response of Metal Oxide Sensors to DMMP

•WO_3 powders by Kim et al., Sensors and Actuators B 76, 442 (2001)

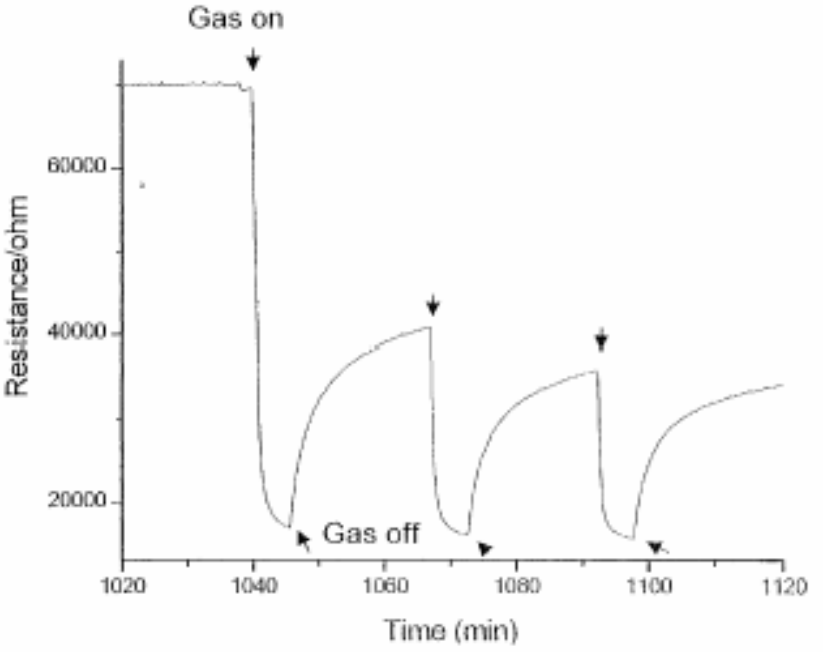

•SnO_2 nanobelt-MEMS sensor

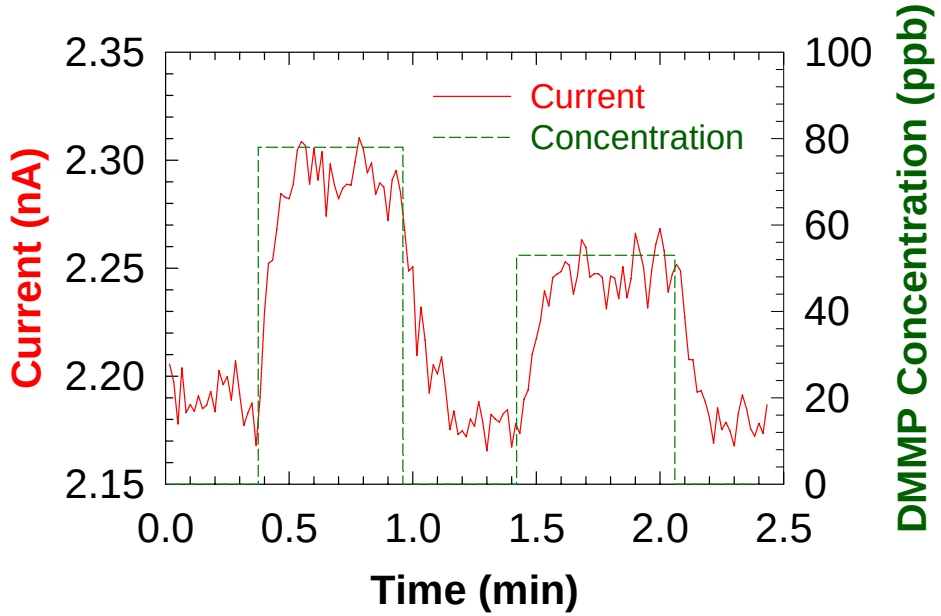

•At above 300°C, a covalently-bonded, stable phosphate surface complex adsorbed on TiO_2 and WO_3 surface was thought to cause the sensor poisoning

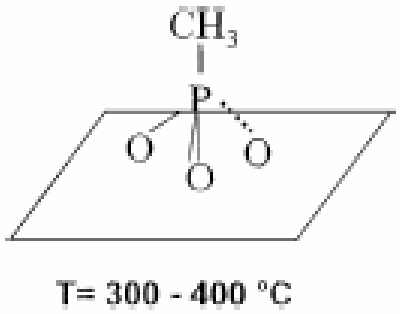

- The sensor temperature was increased to 500°C by the MEMS heater
- High sensitivity: 10-100 ppb
- Full recovery upon purging the sensor with air, no sensor poisoning.
- Result of the single crystal structure or Pt catalytic sites from FIB Pt deposition?

Future Work

• To better understand the effects of crystal structure, nanobelt thickness, catalytic additives, operating temperatures, and contact metals on sensor sensitivity, stability, response time, and dynamic range.

• To further develop methods for wafer-scale fabrication of selective microsensor arrays containing multiple layers of different metal oxide nanowire sensing elements doped with catalytic additives:

- Langmuir-Blodgett assembly of aligned nanowire monolayers + photolithography & patterning

- Microsensor arrays containing 3D interconnected nanowire networks

• 3D interconnected WO_3 nanowire network (Z. L. Wang and co-workers)

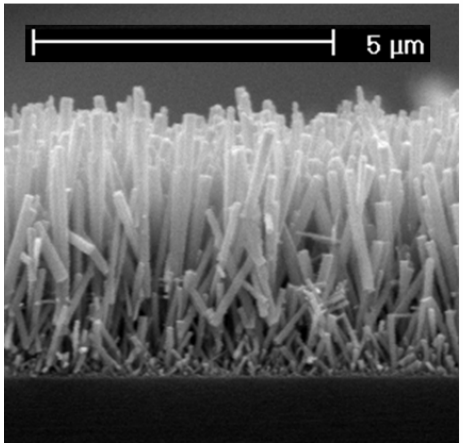

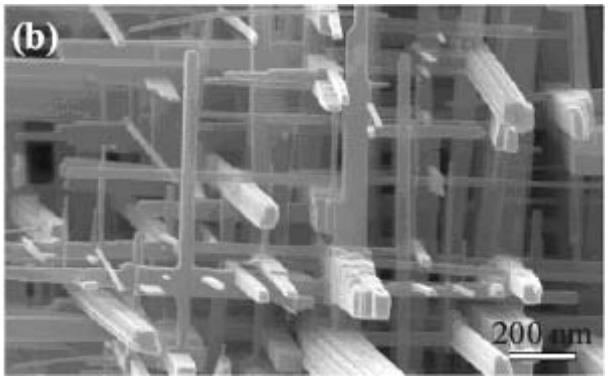

Acknowledgment

Post-doc & Grad Students:

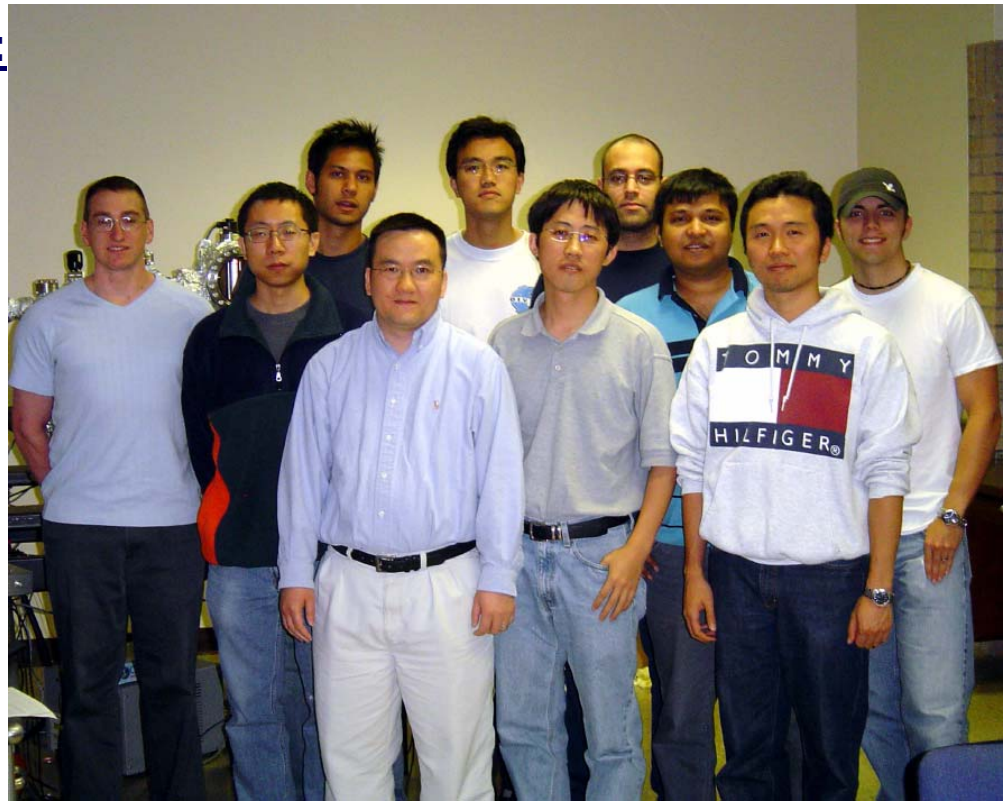

Collaborations:

- A. Gossard Group
- S. Jin Group
- X. G. Li Group
- A. Majumdar Group
- N. Mingo & Q. Ye
- R. Ram Group
- A. Shakouri Group
- C. K. Shih Group
- Z. L. Wang Group
- Z. Yao Group

Research Sponsors:

ONR (Program Manager: Dr. Mihal E. Gross)

NSF Thermal Systems Program

NASA / Eloret

DARAPA AP2C

THECB Advanced Research Program